Effect of dispersion on the nanoscale patterns produced by ion sputtering

Kevin M. Loew and R. Mark Bradley

Phys. Rev. E **100**, 012801 — Published 24 July 2019

DOI: 10.1103/PhysRevE.100.012801

The Effect of Dispersion on the Nanoscale Patterns Produced by Ion Sputtering

Kevin M. Loew

Department of Physics, Colorado State University, Fort Collins, CO 80523, USA

R. Mark Bradley

Departments of Physics and Mathematics,

Colorado State University, Fort Collins, CO 80523, USA

(Dated: July 3, 2019)

Abstract

Our simulations show that dispersion can have a crucial effect on the patterns produced by oblique-incidence ion sputtering. It can lead to the formation of raised and depressed triangular regions traversed by parallel-mode ripples, and these bear a strong resemblance to nanostructures that are commonly observed in experiments. In addition, if dispersion and transverse smoothing are sufficiently strong, highly ordered ripples form. Finally, dispersion can cause the formation of protrusions and depressions that are elongated along the projected beam direction even when there is no transverse instability. This may explain why topographies of this kind form for high angles of ion incidence in cases in which ion-induced mass redistribution is believed to dominate curvature-dependent sputtering.

I. INTRODUCTION

Bombarding a solid surface with a broad ion beam can produce a remarkable variety of self-assembled nanoscale patterns, including periodic height modulations and mounds arranged in hexagonal arrays of surprising regularity [1–6]. The spontaneous formation of these patterns is not just fascinating in its own right: Ion bombardment has the potential to become a cost-effective method to rapidly fabricate large-area nanostructures with features smaller than those that can be produced by conventional optical lithography.

The first type of pattern formation to be discovered was the ripples that often develop when the nominally flat surface of an elemental solid is bombarded with an obliquely-incident noble gas ion beam [1, 7]. According to the Bradley-Harper (BH) theory [8], this is the result of a surface instability caused by the curvature dependence of the sputter yield: The sputter yield is greater in a trough than at a crest. The selected ripple wave vector $\boldsymbol{k}$ has the highest growth rate, and results from the competition between the destabilizing effect of sputtering and the smoothing effect of surface diffusion.

In the BH theory, the amplitude of the surface disturbance increases exponentially in time. To account for the saturation in the amplitude of the ripples that is observed experimentally, the leading order nonlinear terms must be added to the linear BH equation of motion [9]. After transforming to an appropriately chosen moving frame of reference, this gives the anisotropic Kuramoto-Sivashinsky (KS) equation

$$u_t = C_{11}u_{xx} + C_{22}u_{yy} - B\nabla^2\nabla^2 u + \lambda_1 u_x^2 + \lambda_2 u_y^2, \tag{1}$$

where $u(x, y, t)$ is the height of the surface above the point (x, y) in the $x - y$ plane at time t; the subscripts x, y, and t denote partial derivatives; the direction of the incident ions has polar angle $\theta \geq 0$ and zero azimuthal angle; $\nabla^2 \equiv \partial_x^2 + \partial_y^2$ and B is the surface diffusivity. The constants C_{11}, C_{22}, λ_1 and λ_2 depend on the angle of incidence of the ion beam θ and were originally computed using the Sigmund theory of sputtering [8, 10, 11]. If $C_{11} < C_{22}$ and $C_{11} < 0$, ripples with their wave vector parallel to the surface projection of the ion beam direction form; these are called parallel-mode ripples. Conversely, if $C_{22} < C_{11}$ and $C_{22} < 0$, perpendicular-mode ripples emerge.

It is now known that the values of the coefficients C_{11} and C_{22} are influenced not just by sputtering but by ion-induced mass redistribution [13–15] and ion implantation [16, 17]

as well. In addition, for the temperatures typically used in experiments, the predominant contribution to the term $-B\nabla^2\nabla^2 u$ in Eq. (1) is ion-induced viscous flow near the surface of the solid rather than thermally activated surface diffusion [18].

In the original BH theory, the Sigmund model of ion sputtering was reduced to a partial differential equation for a nearly flat surface with slowly varying surface height [8]. The dependence of the sputter yield on the surface curvature (i.e., on second derivatives of the surface height u) was included in the theory, but its dependence on third and higher order spatial derivatives of u was omitted. Makeev, Cuerno and Barabási extended the BH analysis to include terms proportional to third order spatial derivatives of u as well as other, higher order terms which we shall omit [11]. The resulting equation of motion is

$$u_t = C_{11}u_{xx} + C_{22}u_{yy} - B\nabla^2\nabla^2 u + \lambda_1 u_x^2 + \lambda_2 u_y^2 + C_{111}u_{xxx} + C_{122}u_{xyy}. \tag{2}$$

For a surface with slowly varying height, u_{xxx} and u_{xyy} are in general larger than $\nabla^2\nabla^2 u$, and so it is actually inconsistent to omit the third-order terms.

The simplest and most obvious effect of including terms proportional to u_{xxx} and u_{xyy} in the equation of motion (EOM) is that it makes the ripple propagation dispersive [11, 12]. There is direct experimental evidence that establishes that the effect of dispersion can be substantial [19]. The dispersive terms in Eq. (2) can result from ion-induced plastic flow [20, 21] or viscous relaxation of ion-induced stresses [22, 23] as well as from sputtering [11, 24].

In this paper, we will explore the effects of dispersion on the patterns produced by oblique-incidence ion sputtering. We find that dispersion can lead to the formation of raised and depressed triangular regions that are traversed by parallel-mode ripples. These regions — which we will often refer to as "triangles" for the sake of brevity — strongly resemble structures that are commonly observed in experiments. In a different range of the model's parameters, highly ordered ripples emerge. This suggests that dispersion could be employed to produce much more orderly ripples than those that are usually found in experiments. Finally, protrusions and depressions that are elongated in the longitudinal direction can emerge at sufficiently long times. These topographies resemble the so-called perpendicular-mode ripples that are frequently observed for high angles of ion incidence.

This paper is organized as follows. We study the behavior of the surface for the special case in which its height does not depend on the transverse coordinate y in Sec. II. The

general case in which u depends on x, y and t is considered in Sec. III. We put our results in context in Sec. IV and discuss them further in Sec. V. Our conclusions are presented in Sec. VI.

II. RIPPLE FORMATION IN ONE DIMENSION

Consider a one-dimensional (1D) disturbance (i.e., one with $u_y = 0$ everywhere) and suppose that $C_{11} < 0$ so that there is an instability. We introduce the dimensionless quantities $\tilde{x} = \mathrm{sgn}(C_{111})(|C_{11}|/B)^{1/2}x$, $\tilde{t} = (C_{11}^2/B)t$ and $\tilde{u} = (\lambda_1/|C_{11}|)u$, where $\mathrm{sgn}(C_{111})$ denotes the sign of C_{111}. After dropping the tildes, we obtain the rescaled equation of motion

$$u_t = -u_{xx} - u_{xxxx} + u_x^2 + \alpha u_{xxx}, \tag{3}$$

where $\alpha \equiv (B|C_{11}|)^{-1/2}|C_{111}|$ is a nonnegative, dimensionless measure of the strength of the dispersion. In the new, rescaled coordinate system, the projection of the ion beam onto the $x - y$ plane points in the $-x$ direction if $C_{111} > 0$, while if $C_{111} < 0$, it points in the $+x$ direction.

For $\alpha = 0$, Eq. (3) reduces to the one-dimensional KS equation. In this limit, solutions to Eq. (3) with low-amplitude spatial white noise initial conditions exhibit spatio-temporal chaos.

We differentiate Eq. (3) with respect to x and set $\bar{x} = -x$, $\bar{t} = \alpha t$ and $v = (2/\alpha)u_x$. After dropping the bars, we have

$$v_t + \alpha^{-1}(v_{xx} + v_{xxxx}) + vv_x + v_{xxx} = 0. \tag{4}$$

Equation (4) is known as the Kawahara equation [25] and has previously been studied as a model of step-bunching dynamics on vicinal surfaces [26, 27]. It reduces to the Korteweg-Vries (KdV) equation

$$v_t + vv_x + v_{xxx} = 0, \tag{5}$$

a paradigmatic equation in the study of solitons, in the strongly dispersive limit $\alpha \to \infty$. When α is large and finite and the initial condition is low-amplitude spatial white noise, the solution to Eq. (4) tends to a highly ordered steady state that consists of a chain of equally-spaced solitons of the same amplitude [25].

We numerically integrated Eq. (3) using the fourth-order Runge-Kutta exponential time-differencing (ETD4RK) method described by Cox and Matthews [28]. This integration scheme utilizes periodic boundary conditions. The linear terms of the equation were computed exactly in Fourier space; on the other hand, the nonlinear terms were approximated in real space using finite differencing. A central difference scheme accurate to fourth order in the grid spacing along the x direction, Δx, was used for the derivatives. In particular, the partial derivative of u with respect to x was approximated by [29]

$$\left.\frac{\partial u}{\partial x}\right|_{x_i} \cong \frac{-u_{i+2} + 8u_{i+1} - 8u_{i-1} + u_{i-2}}{12\Delta x}. \tag{6}$$

Figure 1 shows the results of simulations for a selection of α values at time $t = 300$. In each case, the initial condition was low amplitude spatial white noise. (The amplitude of the white noise was chosen to be 0.01 for all simulations discussed in this paper.) For $\alpha = 0$, Eq. (3) is the 1D KS equation and the solution exhibits spatial-temporal chaos. The dispersive term seems not to fundamentally alter the behavior for $\alpha = 0.1$. However, for $\alpha = 0.5$, the ripples are much closer to being periodic. For $\alpha = 1$, sections of the surface have well-ordered ripples superimposed on an overall upward slope. These sections are followed by precipitous downward drops. The order increases still further for larger values of α until, for $\alpha = 25$, the ripples are almost perfectly ordered but are modulated by a low amplitude, long wavelength height variation. For still larger values of α, the modulation is of smaller amplitude, and the highly ordered steady state can be thought of as a chain of equally-spaced solitons of the same amplitude, as noted above [25].

To quantify the increase in order with increasing α, we generated a new set of simulations. Simulations were carried out for a range of values of α between 0.1 and 40 on a domain of width 10000, and for each value of α, ten independent simulations were generated with low amplitude spatial white noise initial conditions. We then took the absolute value of the Fourier transform of each of the surfaces corresponding to a single α value at time $t = 800$ and averaged. We next fit a Gaussian to the first peak of the averaged curve and calculated the full width at half max (FWHM) of the Gaussian. As usual, the smaller the FWHM, the more orderly the surface is. Figure 2 (a) indeed shows that as α increases, the FWHM of the fitted Gaussian decreases.

The location of the Gaussian's peak yields the wavelength of the ripples at time $t = 800$, a time when a steady state has very nearly been reached. As shown in Fig. 2 (b), the ripple

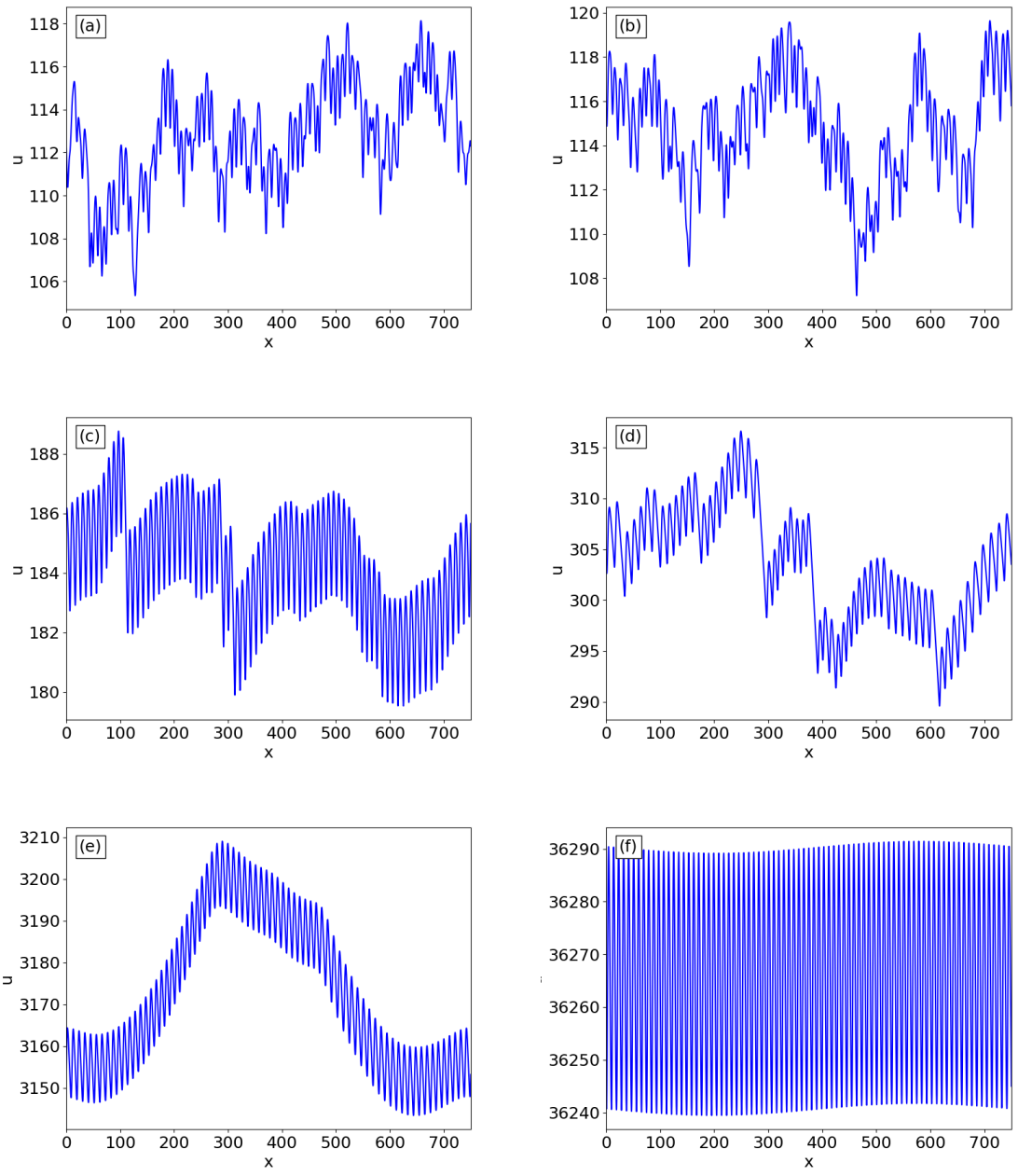

FIG. 1: (Color online) u versus x at time $t = 300$ for (a) $\alpha = 0$, (b) $\alpha = 0.1$, (c) $\alpha = 0.5$, (d) $\alpha = 1$, (e) $\alpha = 5$ and (f) $\alpha = 25$. The domain width was 750.

wavelength Λ depends on α at $t = 800$. In contrast, the wavelength at early times takes on the linearly-selected value $2\sqrt{2}\pi$, which is independent of α. This means that the ripple wavelength must in general depend on time. This time dependence is illustrated in Fig. 3 for $\alpha = 2$, 10, 25, and 50. Importantly, the wavelength at long times exceeds the linearly selected value for all values of α we examined, which means that the dispersive term produces

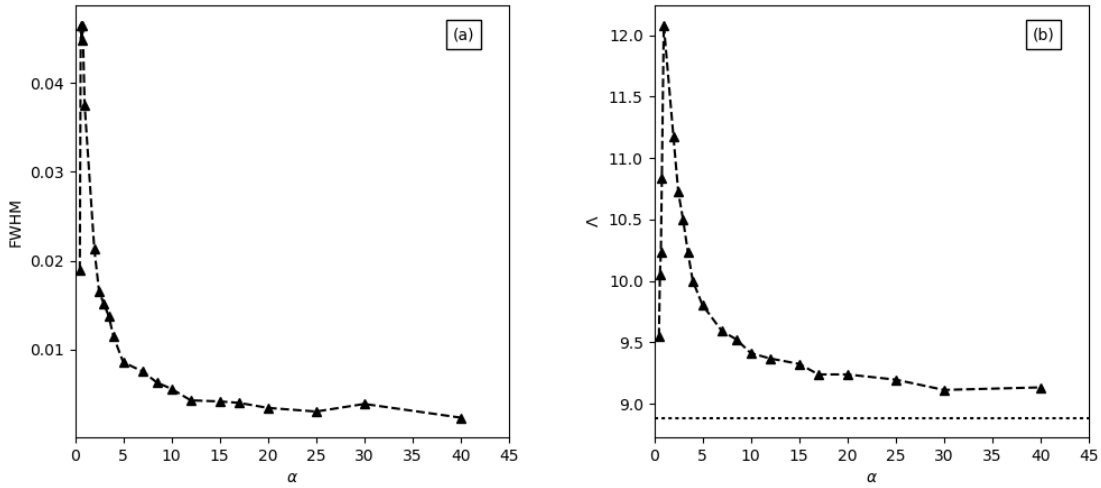

FIG. 2: (a) The full width at half max (FWHM) and (b) wavelength Λ versus α at time $t = 800$. The dashed black lines are guides to the eye, the triangles are the actual points calculated, and the dotted line in (b) displays the linearly selected wavelength $2\sqrt{2}\pi$. The domain width was 10000.

ripple coarsening. This coarsening is interrupted, i.e., it does not continue indefinitely. Our simulations suggest that the long-time value of Λ tends to the linearly-selected value $2\sqrt{2}\pi$ in the $\alpha \to \infty$ limit.

An interesting feature that is not apparent in Fig. 1 is the asymmetry of the ripple pattern for nonzero α. Figure 4 shows a portion of the surface for $\alpha = 1$ at time $t = 300$. The right and left sides of the ripple crest shown in the figure are clearly different. This is to be expected since Eq. (3) is not invariant under the transformation $x \to -x$ for $\alpha > 0$.

It is natural to ask whether the effects of dispersion could be observed in an experiment. For a typical material, $C_{11} = C_{11}(\theta)$ changes sign from positive to negative as θ is increased from zero through a critical angle θ_c. Ripples form for θ just above θ_c and the dimensionless measure of the strength of the dispersion $\alpha = (B|C_{11}|)^{-1/2}|C_{111}|$ is large in this regime. When C_{11} is small and negative, however, the characteristic time B/C_{11}^2 that it takes for the ripple amplitude to become appreciable is large. This means that an unattainably high fluence might be needed for ripples to form and for the effects of dispersion to become noticeable. Fortunately, α need not be large for the effects of dispersion to be substantial. If α is of order 1, our simulations show that the behavior of the surface is strongly affected

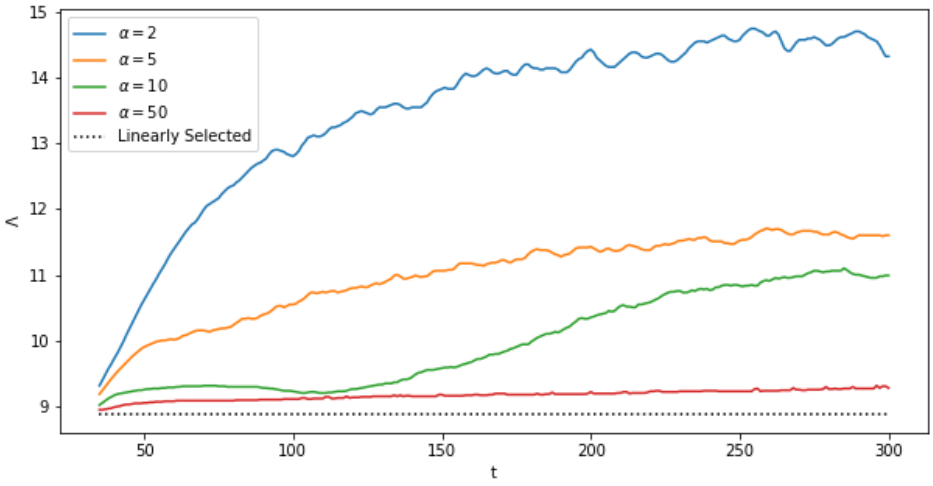

FIG. 3: (Color online) Wavelength versus time for $\alpha = 2$, 5, 10, and 50. The dotted black line shows the linearly-selected wavelength. The domain width was 10000.

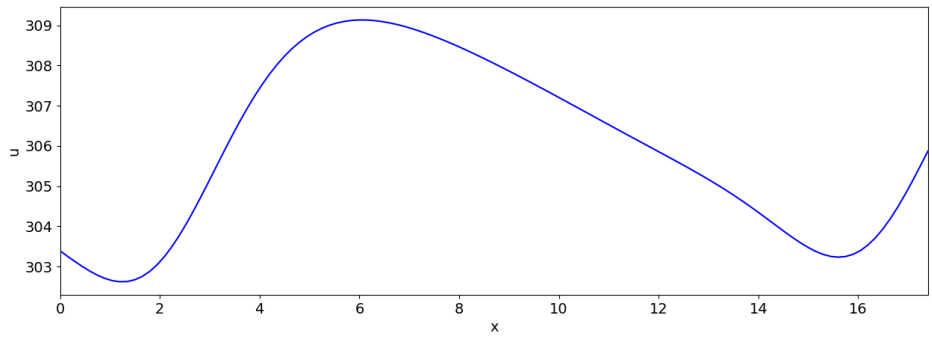

FIG. 4: (Color online) u versus x at time $t = 300$ for $\alpha = 1$.

by dispersion when times are reached that are several hundred times the characteristic time B/C_{11}^2 [see Fig. 1 (d)]. Times this long are commonly reached in experiments.

III. PATTERN FORMATION IN TWO DIMENSIONS

As we have seen, the dispersive term has a significant effect on the surface produced by Eq. (2) for the special case in which u is independent of the transverse coordinate y. However, there are variations in height in both the longitudinal and transverse directions in experiments, and so we must consider the behavior predicted by the full equation of motion

(2) when u depends on x, y, and t. This will henceforth be called the two-dimensional (2D) case.

We begin by defining $\tilde{x}$, $\tilde{t}$ and $\tilde{u}$ as in Sec. II and by setting $\tilde{y} = (|C_{11}|/B)^{1/2}y$. We once again assume that C_{11} is negative so that an instability is present in the longitudinal direction. After dropping the tildes, Eq. (2) becomes

$$u_t = -u_{xx} + r_1 u_{yy} - \nabla^2\nabla^2 u + u_x^2 + r_2 u_y^2 + \alpha u_{xxx} + \beta u_{xyy}, \tag{7}$$

where $r_1 \equiv C_{22}/|C_{11}|$, $r_2 \equiv \lambda_2/\lambda_1$ and $\beta \equiv (B|C_{11}|)^{-1/2}C_{122}$ are dimensionless parameters and we remind the reader that $\alpha \equiv (B|C_{11}|)^{-1/2}C_{111}$.

A. Highly Ordered Ripples

A sensible starting point for the study of the 2D problem is a case that is roughly analogous to the 1D case: we assume that r_1 is positive so that there is no linear instability in the transverse direction. In fact, we will go further and consider the case $r_1 = 10$ in this subsection so that variations in the y direction are rather strongly suppressed.

Just as was done for the 1D special case, a set of simulations were conducted starting from a low-amplitude spatial white noise initial condition. The numerical integrations were once again performed using the ETD4RK method. Several different values of α were considered. The values of the remaining parameters were $r_2 = 1$, $\beta = 0$ and, as already mentioned, $r_1 = 10$.

Figure 5 shows that increasing α promotes the formation of highly ordered ripples, just as in the 1D case. In the absence of dispersion, there is no clear order in the x direction, but as the coefficient of the dispersive term u_{xxx} is increased, order in the x direction starts to emerge and then becomes very strong for large dispersion, e.g., for $\alpha = 50$.

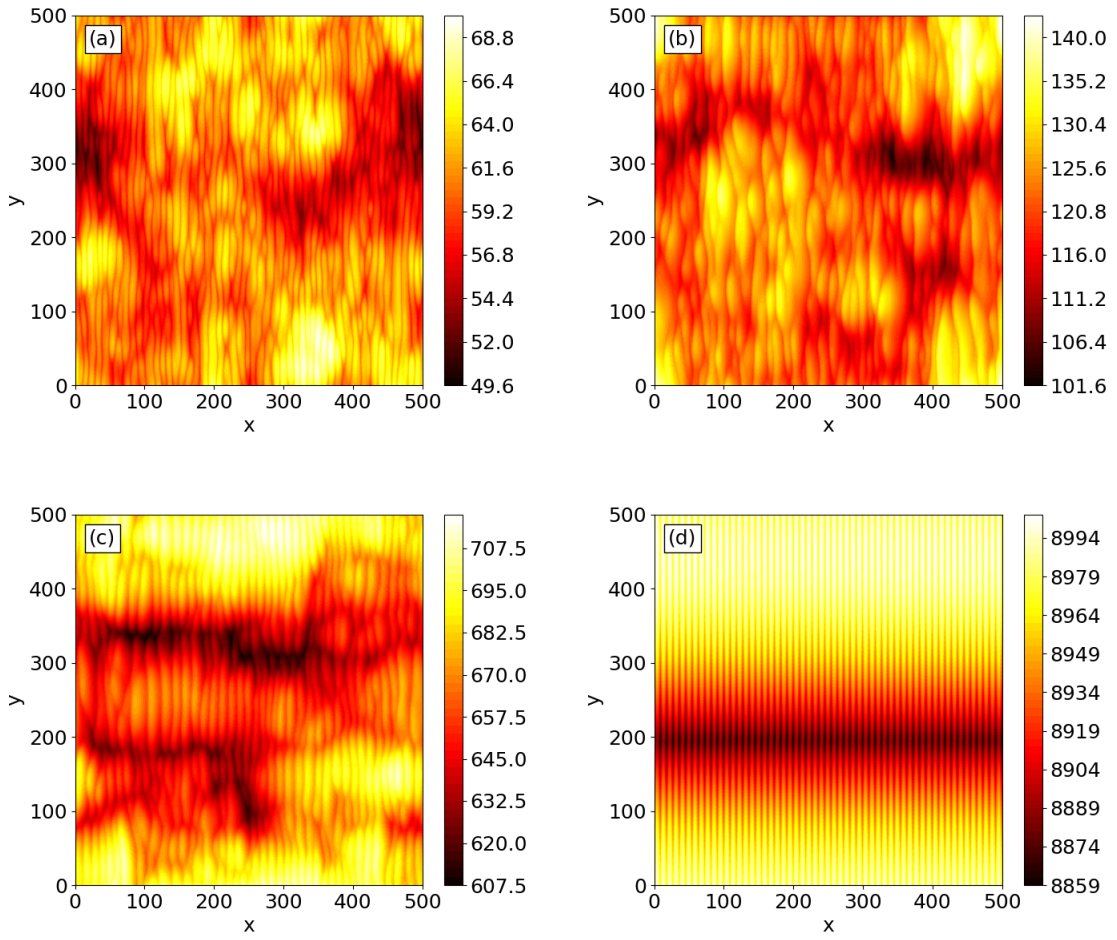

FIG. 5: (Color online) u vs x and y at time $t = 200$ for $r_1 = 10$, $r_2 = 1$, $\beta = 0$ and (a) $\alpha = 0$, (b) $\alpha = 1$, (c) $\alpha = 5$ and (d) $\alpha = 50$. The domain size was 500×500.

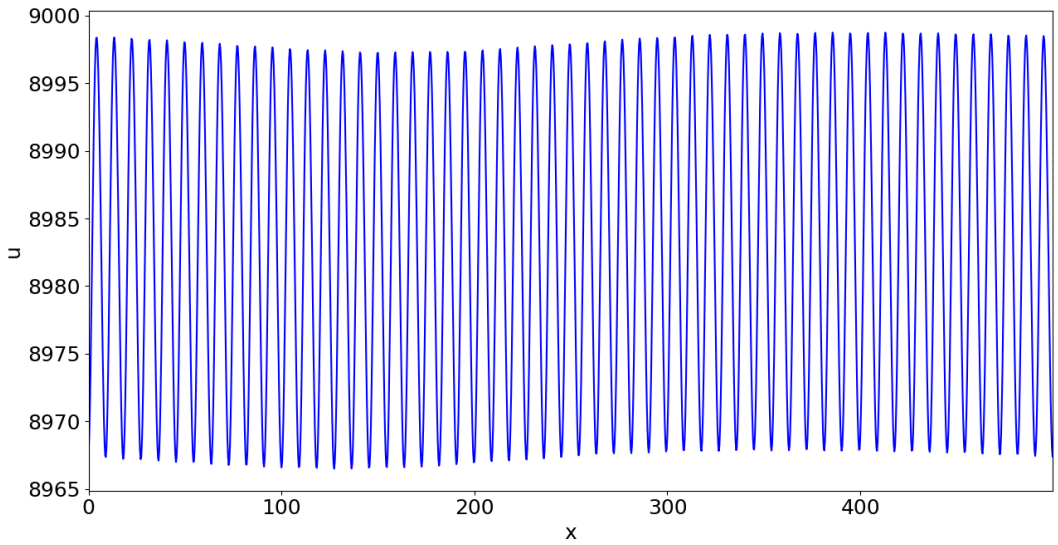

FIG. 6: (Color online) Cross section of the simulation shown in Fig. 5 (d) at $y = 400$.

Figure 6 shows that a one-dimensional cross section of the surface with $\alpha = 50$ is qualitatively similar to the result of the 1D simulation with $\alpha = 25$ that is displayed in Fig. 1 (f). Both simulations produce highly ordered ripples with a minor long-wavelength modulation in the x-direction.

Although the surface is highly ordered in the x direction in Fig. 5 (d), it is noticeably depressed for y in the vicinity of 200. To see how this kind of feature emerges and what its ultimate fate is, we simulated the time evolution of the surface for the same parameters as in Fig. 5 (d), i.e., $r_1 = 10$, $r_2 = 1$, $\alpha = 50$ and $\beta = 0$, but ran the simulation for a longer period of time. The results are shown in Fig. 7. At early times, the time evolution is well described by the linearized equation of motion and parallel-mode ripples form. As the surface continues to evolve, the nonlinear terms start to have a significant effect. By $t = 80$, multiple band-shaped regions have formed in which the ripples are highly ordered. These bands are roughly aligned with the x-direction. Each pair of adjacent bands is separated by a unique type of defect that we will call a "seam." A seam is depressed relative to its surroundings and the ripples on either side of it may or may not be in phase. In fact, as we trace along a seam, the relative phase of the flanking ripples may change. Comparable but much shorter defects can be found in images of surfaces bombarded with an obliquely incident ion beam [30–33] — see the middle and right panels of Fig. 3 of Ref. [31], for

example.

Figure 8 is a close-up of the time evolution of two seams. As time passes, the two seams near each other and then merge. After this has occurred, the ripples to either side of the one remaining seam are quite close to being in phase, as in Fig. 8 (c). The depression then becomes shallower and at long times the seam disappears for all intents and purposes, very much like the behavior of the seam shown in Fig. 7 (d)-(f). The ripples are highly ordered at that point.

Close examination of Fig. 5 shows that the wavelength is shorter for $\alpha = 50$ than for $\alpha = 5$. To investigate this point, we calculated the peak-to-peak and trough-to-trough separations for a regularly-spaced sequence of 1D cuts through the surface at time $t = 800$. Each of these cuts had a different, fixed value of y. Normalized histograms of the separations for $\alpha = 2$ and $\alpha = 15$ are displayed in Fig. 9. We observe that just as in the 1D case, the mean wavelength is shorter for the larger value of α. For both values of α, the mean wavelength at long times exceeds the linearly-selected wavelength $2\sqrt{2}\pi \cong 8.886$, and so coarsening occurs in the 2D case, as it does in 1D. The distribution of separations is narrower for $\alpha = 15$ than for $\alpha = 2$, which is in accord with our observation that the ripples become more ordered as α is increased.

The ordered ripples generated by strong dispersion is a fascinating phenomenon. However, thus far, we have restricted our attention to the case $\beta = 0$. It is unlikely that β will be exactly zero in an experiment. We therefore carried out simulations in which we again set $r_1 = 10$, $r_2 = 1$ and $\alpha = 50$ but chose β to be ± 10 (see Fig. 10). In both cases, there are regions of highly ordered ripples that are separated by seams, as for $\beta = 0$. For $\beta = 10$, though, the ordered regions are smaller and the seams are more abundant than for $\beta = 0$ or -10.

B. Triangular Structures

To this point, we have considered systems that either have no variation or that are strongly stabilizing in the transverse direction. (r_1 is relatively large and positive in the latter case.) In both of these cases, the presence of the dispersive term αu_{xxx} greatly alters the behavior of the surface when α is sufficiently large: the behavior changes from spatio-temporal chaos in the absence of dispersion to highly ordered ripples in the highly dispersive case. However,

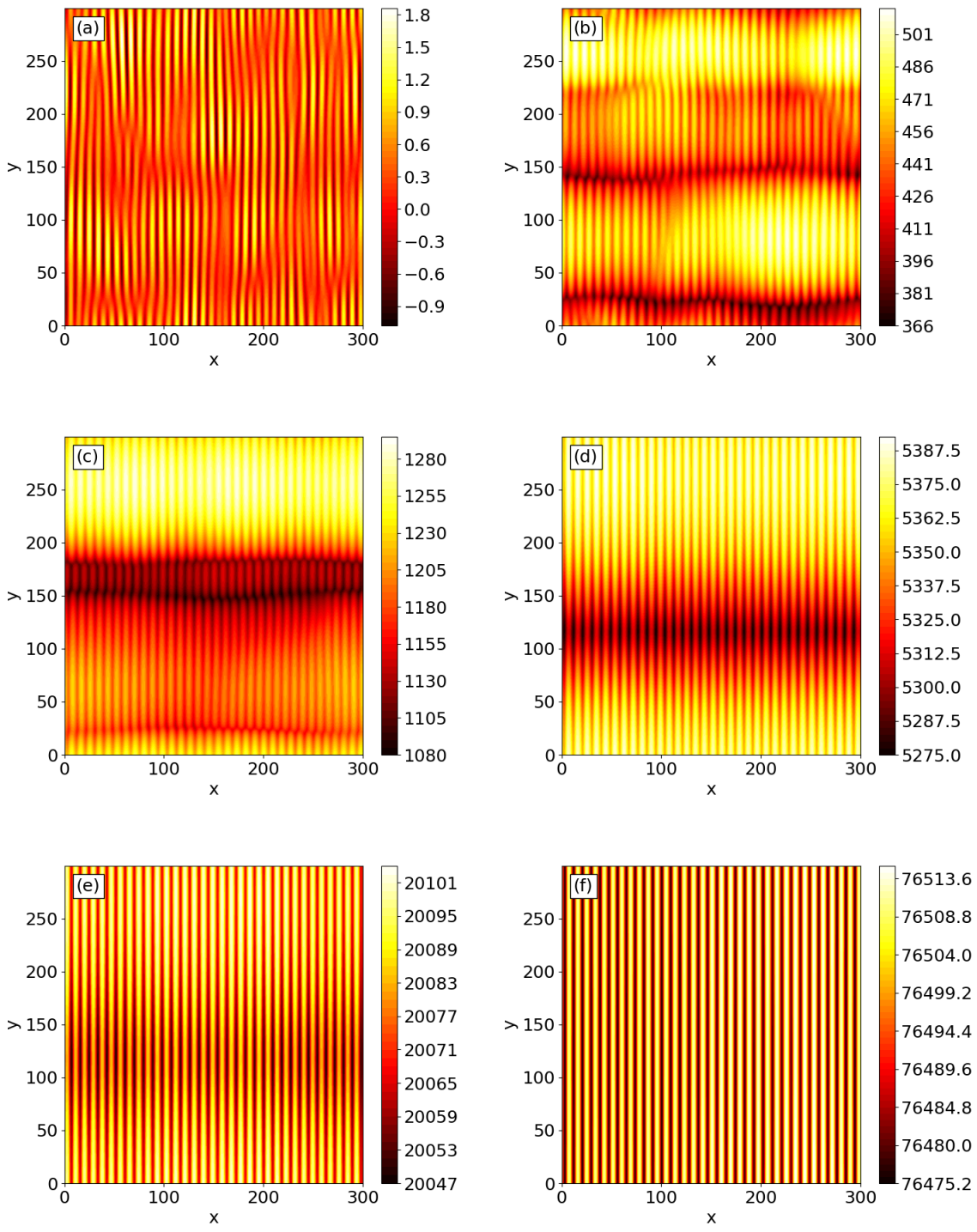

FIG. 7: (Color online) u vs x and y for $r_1 = 10$, $r_2 = 1$, $\alpha = 50$ and $\beta = 0$ for times (a) $t = 50$, (b) $t = 70$, (c) $t = 80$, (d) $t = 130$, (e) $t = 310$, and (f) $t = 1000$. The domain size was 300×300.

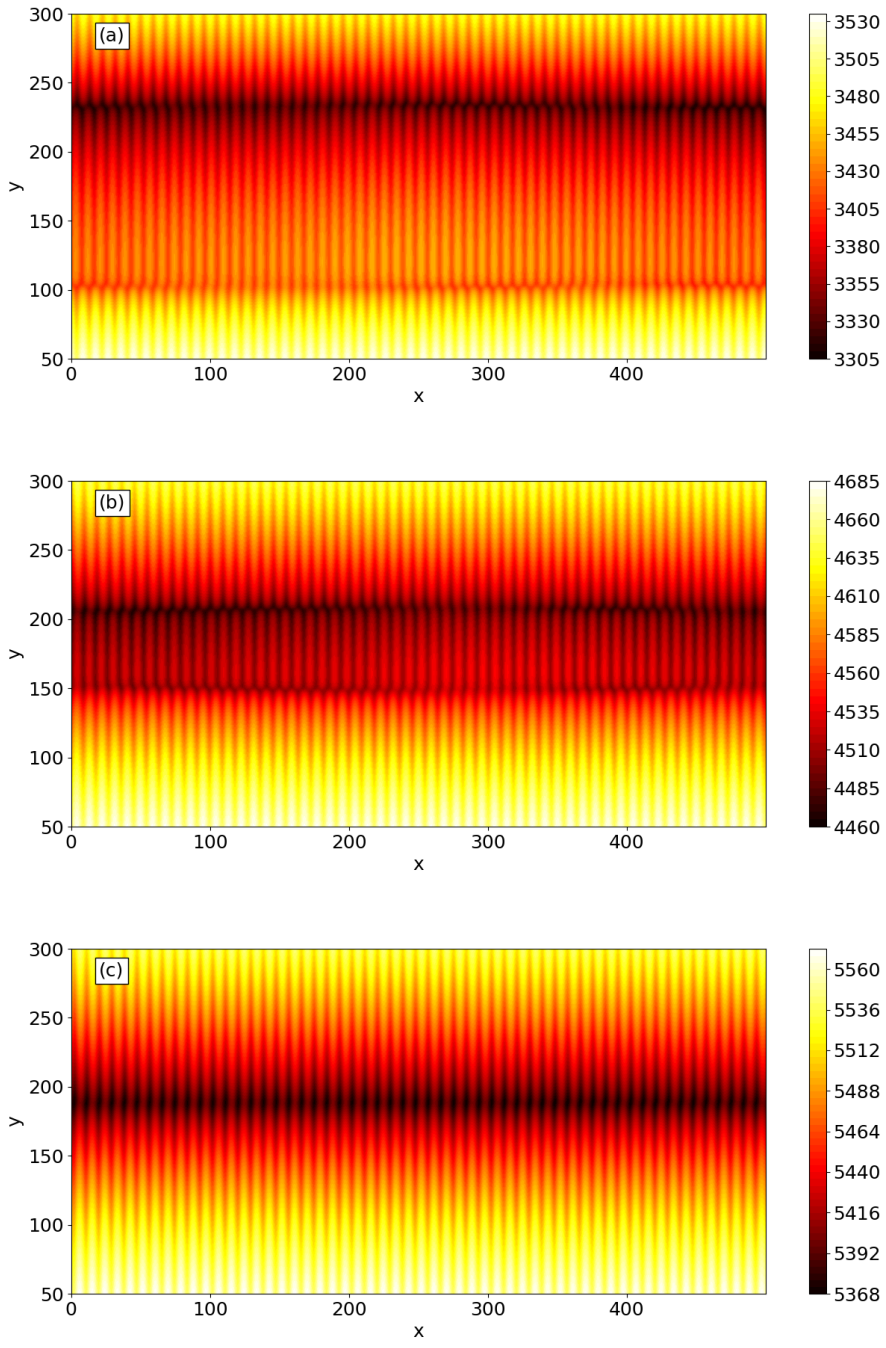

FIG. 8: (Color online) u vs x and y for $r_1 = 10$, $r_2 = 1$, $\alpha = 50$ and $\beta = 0$ for times (a) $t = 114$, (b) $t = 132$, and (c) $t = 146$. The simulation domain size was 500×500, but the displayed interval is $50 \leq y \leq 300$ to highlight the seams.

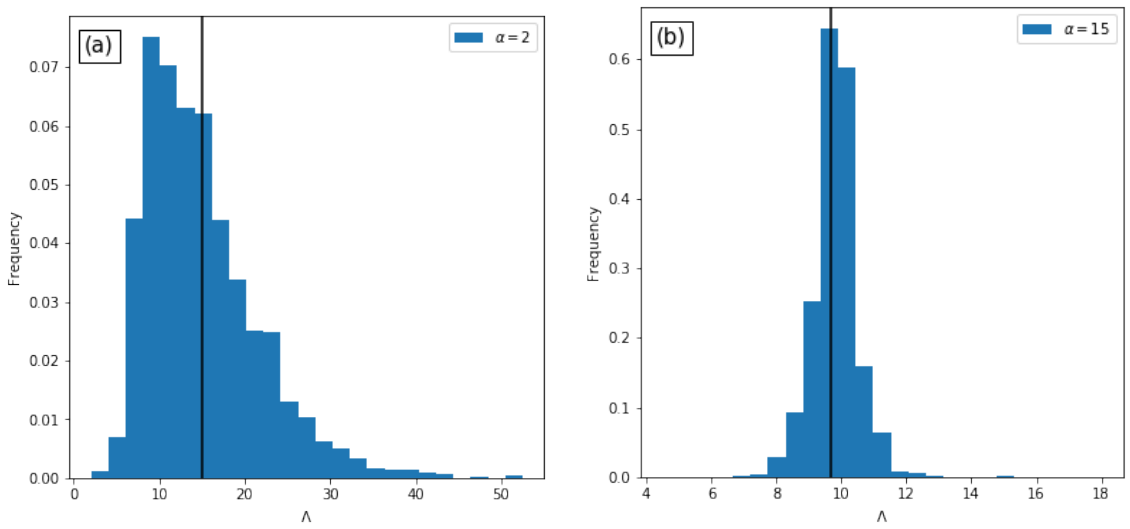

FIG. 9: (Color online) Normalized histograms of the peak-to-peak and trough-to-trough separations along the x direction for (a) $\alpha = 2$ and (b) $\alpha = 15$. The black lines display the mean of the distributions. The mean value is 15.096 for $\alpha = 2$ and 9.684 for $\alpha = 15$.

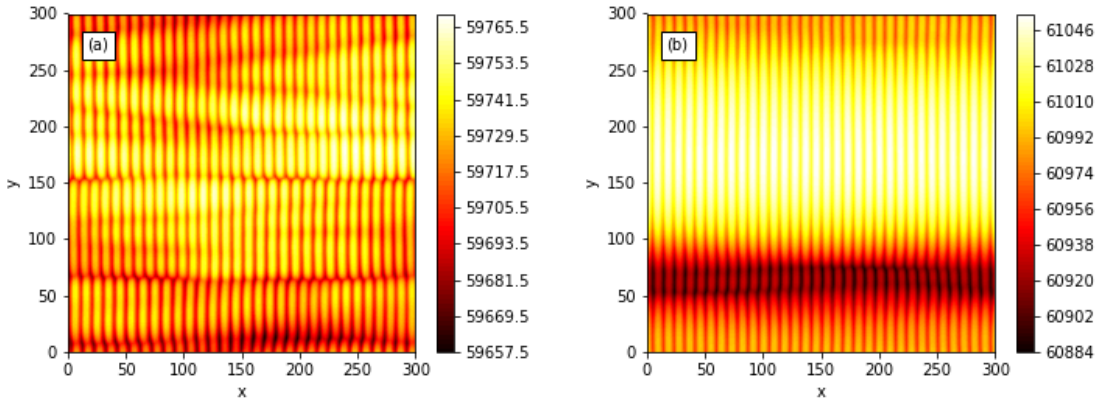

FIG. 10: (Color online) u vs x and y at $t = 200$ for (a) $\beta = 10$ and (b) $\beta = -10$. The remaining parameters were $r_1 = 10$, $r_2 = 1$ and $\alpha = 50$ and the domain size was 300×300.

if the angle of incidence is not too high, r_1 is typically of order 1 and positive. To analyze this situation, we generated a new set of simulations with the parameters $r_1 = 1$, $r_2 = 0$, $\beta = 0$, and with a range of α values. The choice $r_1 = 1$ yields stabilization in the transverse direction, but not to the same degree as previously considered.

The simulations presented in Fig. 11 once again show that the behavior changes fundamentally when α is sufficiently large in magnitude. The most interesting feature that

is observed in these simulations are the triangular structures that emerge for intermediate values of α: see Fig. 11 (c) - (e). Comparable features have been observed in numerous experiments [1, 34–43]; Fig. 3(c) of Ref. [1] is a particularly beautiful example. In both experimental results and in our simulations, triangular structures with parallel-mode ripples superimposed on them appear. These structures come in two varieties: those that protrude out of the surface and those that are depressed below the surrounding region. The raised triangular structures are invariably oriented in one direction while the depressed triangles are oriented in the opposite direction. Furthermore, the two varieties do not form with a one-to-one ratio: there are a larger number of raised triangles than depressed ones in our simulations and in experiments.

For the range of α values in which we do observe triangular structures, they are transient. Figure 12 shows the surface before the emergence of triangles [panel (a)], while triangles are present [panels (b) and (c)], and after they have disappeared [panel (d)]. Figure 12 panels (e) - (h) show the corresponding power spectral densities (PSDs). The PSD is defined to be the squared modulus of the Fourier transform of the difference between the surface height and its spatial average. Before the triangular structures emerge, we see parallel-mode ripples and the corresponding PSD has two peaks centered on nonzero wave vectors on the k_x axis. When triangles are present, these peaks are broader and lower. The PSDs have a distinctive "butterfly" appearance in this regime. The surface at long times appears to exhibit spatio-temporal chaos and there are no discernible peaks in the Fourier spectrum aside from the one centered at $\mathbf{k} = 0$. There are raised and depressed regions on the surface that are elongated along the x-direction at these times.

To further explore the changing nature of the surface morphology, we computed the 1D PSDs for a regularly-spaced sequence of 1D cuts through the surface. Each of these cuts had a different, fixed value of y. We then averaged these PSDs together to give the average 1D PSD for the x direction. We computed the average 1D PSD for the y direction in a completely analogous fashion, except that in this case the 1D cuts had fixed values of x. The results obtained for the same simulation as is shown in Fig. 12 are displayed in Fig. 13 for times $t = 70$ and $t = 500$. These times were selected because triangles were present at the earlier time but not at the later. The average 1D PSDs for the x direction have a strong peak at $t = 70$ but not at $t = 500$. Thus, ripples were present only at the earlier of the two times. The average 1D PSDs for the y direction show that there was no periodicity in the

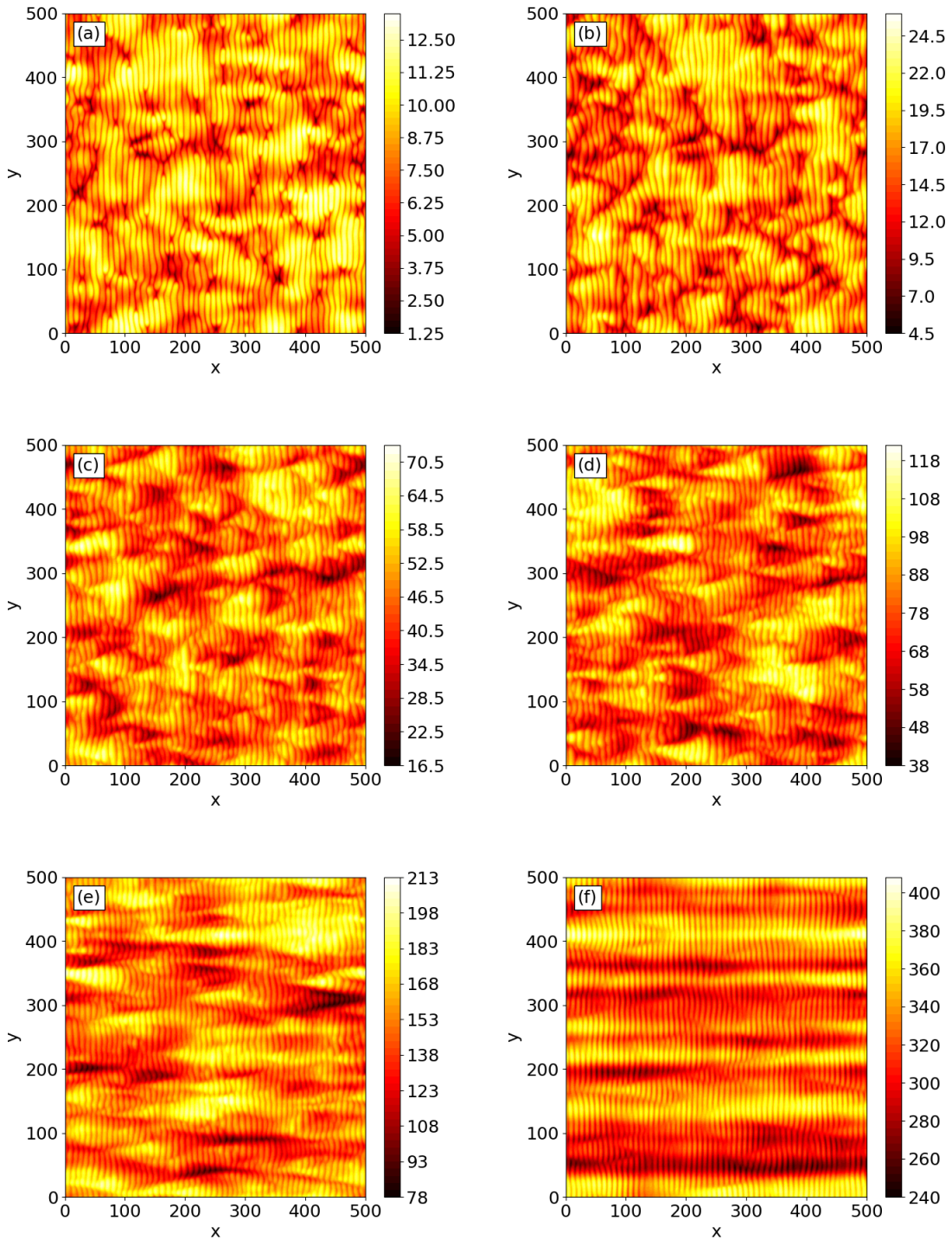

FIG. 11: (Color online) u vs x and y at $t = 60$ for (a) $\alpha = 0$, (b) $\alpha = 1$, (c) $\alpha = 3$, (d) $\alpha = 5$, (e) $\alpha = 10$, and (e) $\alpha = 50$. The remaining parameter values were $r_1 = 1$, $r_2 = 0$ and $\beta = 0$, and the domain size was 500×500.

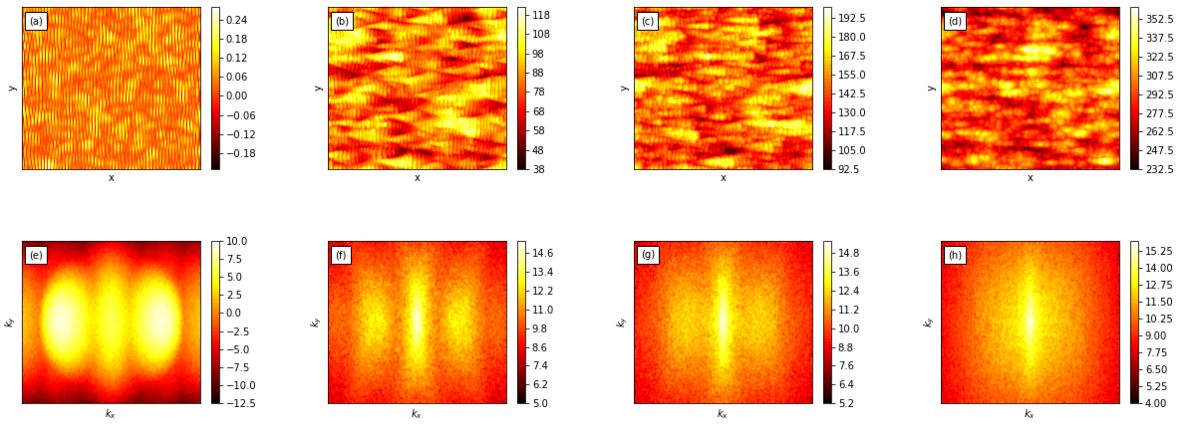

FIG. 12: (Color online) u vs x and y (top) and the corresponding PSDs (bottom) for $r_1 = 1$, $r_2 = 0$, $\alpha = 5$ and $\beta = 0$ for times $t = 32$ [(a) and (e)], $t = 60$ [(b) and (f)], $t = 70$ [(c) and (g)], and $t = 108$ [(d) and (h)]. A logarithmic color scale was used for the PSDs so that the satellite peaks could be seen despite the high central peak. The domain size was 500×500.

y direction for either time.

Figure 14 shows the time dependence of the surface width, i.e., the root-mean-square deviation of the surface height from its mean value, for the same values of α as in Fig. 11. In the linear regime, the surface width grows exponentially with a growth rate that is independent of α. The surface width rapidly saturates as the nonlinear terms become important. The steady-state surface width is an increasing function of α. There is no discernible regime of power-law growth of the surface width at intermediate times.

To this point in this subsection, we have varied α and kept r_2 and β fixed at zero. It is unlikely that that these parameters are exactly equal to zero in experiments, and so we must see if the triangular structures persist in the presence of the terms $r_2 u_y^2$ and βu_{xyy}. We reduced the domain size and ran simulations with $r_1 = 1$ and $r_2 = 0$ once again, but now with two nonzero values of β and fixed $\alpha = 3$. The simulations — which are shown in Fig. 15 (a) and (b) — demonstrate that the additional dispersive term βu_{xyy} alters the detailed structure of the triangles, but they are still present. An additional simulation with $\alpha = 3$, $\beta = 0$, $r_1 = 1$ and $r_2 = 0.2$ shows that the triangles can also form when r_2 is nonzero [see Fig. 15 (c)].

The triangular structures are not invariant under the transformation $x \to -x$. This

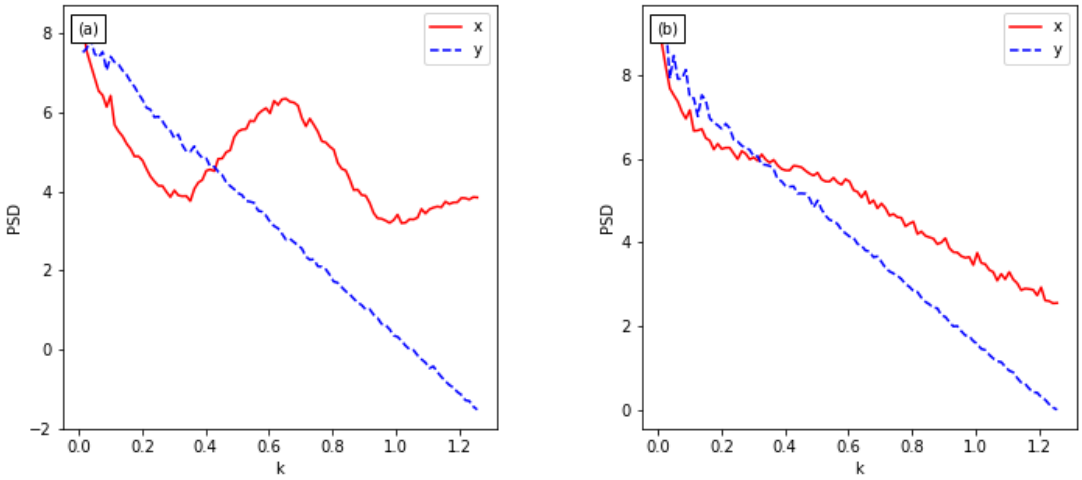

FIG. 13: (Color online) Semilog plots of the averaged PSDs for 1D cuts along the x and y directions are shown for $t = 70$ (a) and $t = 500$ (b). The parameter values were the same as in Fig. 12 and the domain size was 500×500.

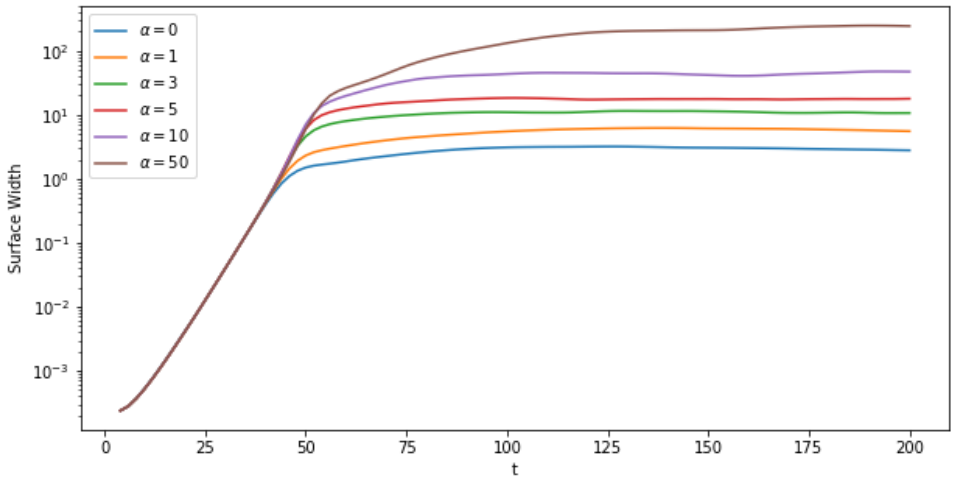

FIG. 14: (Color online) Surface width vs time for $\alpha = 0$, 1, 3, 5, 10, and 50. The remaining parameters were $r_1 = 1$, $r_2 = 0$, and $\beta = 0$. The domain size was 500×500.

symmetry is broken only if α or β or both are nonzero, i.e., dispersive effects are present. Thus, the experimental observation of the formation of triangular structures provides compelling evidence that dispersive effects are significant for many choices of ion beam and

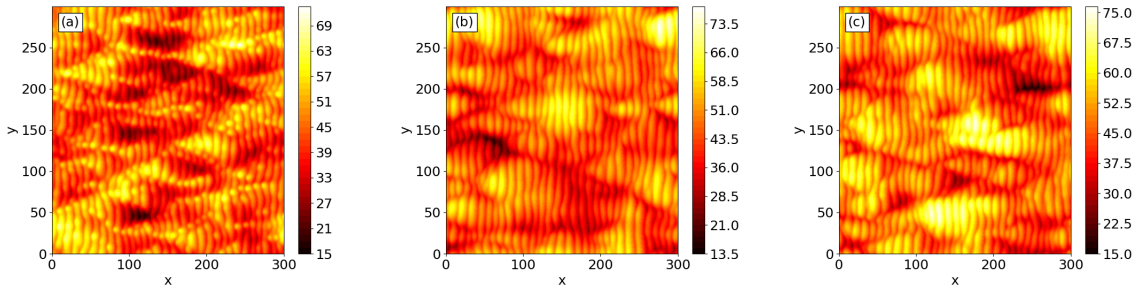

FIG. 15: (Color online) u vs x and y at $t = 60$ for (a) $\beta = 3$ and $r_2 = 0$, (b) $\beta = -3$ and $r_2 = 0$, and (c) $\beta = 0$ and $r_2 = 0.2$. The remaining parameter values were $r_1 = 1$ and $\alpha = 3$. The domain size was 300×300.

target material.

C. Perpendicular-Mode Ripples

The presence of the term αu_{xxx} in our equation of motion (7) makes the ripple propagation dispersive, i.e., ripples with different k_x values propagate with different velocities. This term therefore tends to elongate protrusions and depressions along the x-direction. This tendency is very much in evidence in Fig. 16, which shows the surface height at time $t = 200$ for $r_1 = 1$, $r_2 = 0$ and $\beta = 0$ and for a selection of α values. As α is increased, the protrusions and depressions become increasingly elongated until, for $\alpha = 50$, they span the entire domain. In addition, for $\alpha = 50$, highly ordered, low amplitude parallel-mode ripples are superimposed on the protrusions and depressions. These superimposed ripples are less orderly for smaller values of α.

Protrusions and depressions that are elongated along the x-direction are commonly observed in experiments in which the angle of incidence is relatively high [1]. Traditionally, these have been called perpendicular-mode ripples. According to the linear BH theory [8], perpendicular-mode ripples occur if C_{22} is negative and smaller than C_{11}. In this case, there is an instability in the y-direction and it is stronger than the instability if the x-direction, and $r_1 \equiv C_{22}/|C_{11}| < -1$. The situation is more complex when the equation of motion is taken to be the anisotropic KS equation (1): if $r_1 < -1$ and λ_2/λ_1 is positive and sufficiently small, parallel-mode ripples appear at first but are later supplanted by perpendicular-mode

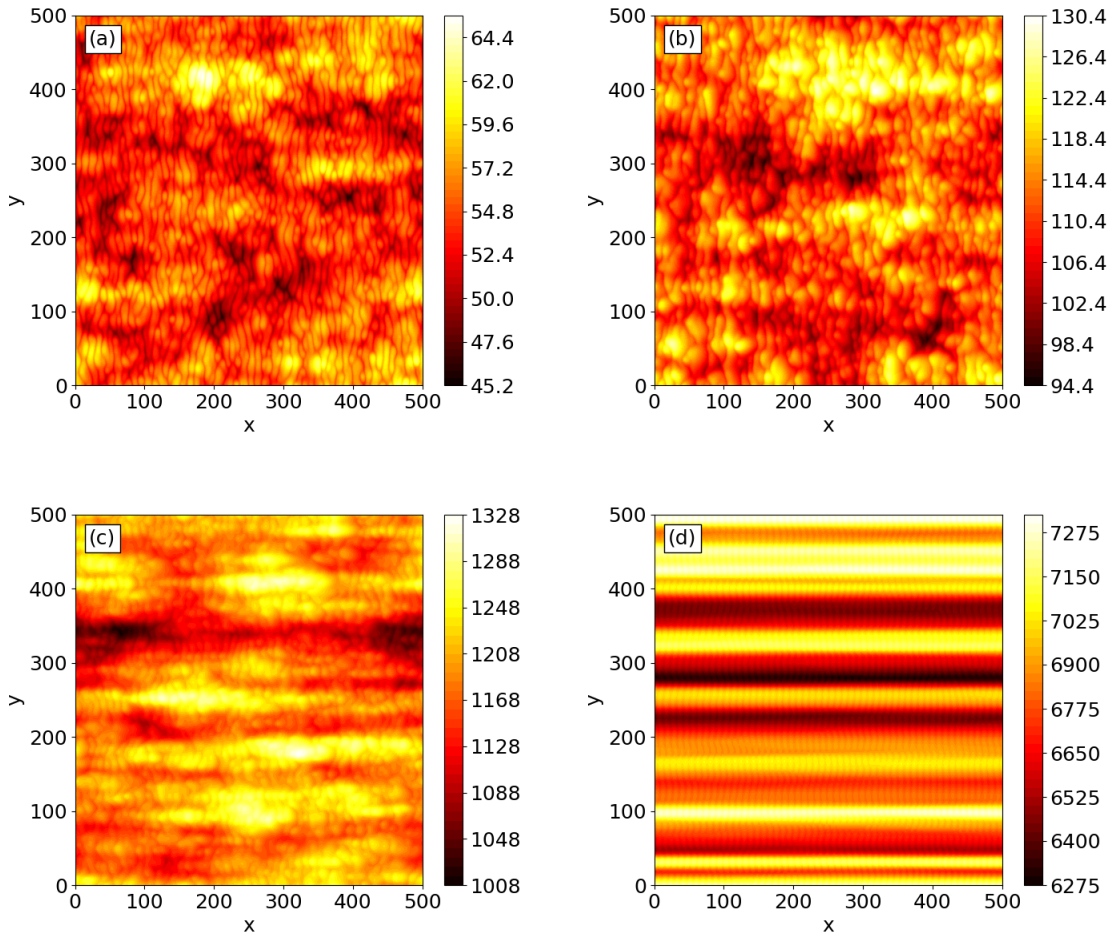

FIG. 16: (Color online) u vs x and y at $t = 200$ for (a) $\alpha = 0$, (b) $\alpha = 1$, (c) $\alpha = 10$, and (d) $\alpha = 50$. In each case, $r_1 = 1$, $r_2 = 0$ and $\beta = 0$. The domain size was 500×500.

ripples [44].

In the simulations that yielded Fig. 16, $r_1 = 1$ and so C_{22} was positive. This means that elongated protrusions and depressions that resemble the experimental topographies can occur even if there is no instability in the y-direction. These topographies are instead the result of dispersion and the lowest-order nonlinearities.

In recent years, atomistic simulations combined with the crater function formalism have been used to estimate the values of the coefficients in the continuum equation of motion [17, 45–47]. These studies have shown that if the ion energy is on the order of 1 keV or smaller, the contribution mass redistribution makes to the curvature coefficients C_{11} and C_{22} is usually about an order of magnitude larger than sputtering's contribution. Mass

redistribution makes a positive contribution to C_{22} [15, 46]. The experimental observation of so-called perpendicular-mode ripples at relatively high angles of incidence has therefore been a puzzle. Our work shows that this apparent quandary may be no quandary at all: adding dispersion and the lowest-order nonlinear terms to the EOM can yield topographies very much like those seen in experiments even if the positive contribution of mass redistribution to C_{22} is larger than negative contribution of curvature-dependent sputtering.

If the angular dependence of the sputter yield is expanded to third order in the surface slope, the cubic nonlinearity u_x^3 appears in the EOM [48]. Recent work has shown that this term can lead to the formation of pyramidal structures that are elongated along the projected beam direction [49]. These too might be considered to be perpendicular-mode ripples. As a consequence, the situation is complex: in a given experiment, so-called perpendicular-mode ripples might result from dispersion, the angular dependence of the sputter yield, from curvature-dependent sputtering, or from a combination of all three.

IV. RELATED WORK

The equation of motion (2) studied in this paper is a special case of the equation derived by Makeev, Cuerno and Barabási (MCB) [11] in which terms proportional to $u_x u_{xx}$ and $u_x u_{yy}$ are omitted and the effective surface diffusivity is taken to be isotropic. MCB only studied the low-amplitude, linearized behavior predicted by their equation.

A still more general equation of motion was derived by Muñoz-García, Cuerno and Castro (MCC) starting from a model in which it is assumed that there is an amorphized, mobile surface layer [12]. Unlike MCB, MCC carried out numerical integrations of their equation of motion in which the nonlinear terms were retained. MCC noted that when terms proportional to u_{xxx} and $u_x u_{xx}$ appear in the EOM, the ripples become asymmetric and their propagation becomes dispersive. They did not observe the formation of triangular structures or highly ordered ripples in 2D, however.

The special case of our rescaled equation of motion (7) in which $r_1 = r_2 = 0$ and $\beta = \alpha$ has already been studied in an entirely different physical context. In this case, much as we did in 1D, we differentiate Eq. (7) with respect to x and set $\bar{x} = -x$, $\bar{y} = y$, $\bar{t} = \alpha t$ and $v = (2/\alpha)u_x$. After dropping the bars, we obtain

$$v_t + \alpha^{-1}(v_{xx} + \nabla^2\nabla^2 v) + v v_x + \nabla^2 v_x = 0. \tag{8}$$

Equation (8) has been studied previously since it models the flow of a thin liquid film down a vertical plane [50]. It reduces to the Kawahara equation (4) if u is independent of the transverse coordinate y.

In the highly dispersive $\alpha \to \infty$ limit, Eq. (8) becomes the 2D version of the Zakharov-Kuznetsov (ZK) equation [51] for ion-acoustic waves propagating along the magnetic field in a strongly magnetized, two-component plasma,

$$v_t + vv_x + \nabla^2 v_x = 0. \tag{9}$$

The ZK equation (9) is a generalization of the KdV equation (5) to 2D. The soliton solutions to the KdV equation are also solutions of the ZK equation. However, these so-called 1D solitons are unstable against perturbations of sufficiently long transverse wavelength [52–56]. When disturbed, a 1D soliton breaks up into a chain of localized, bell-shaped solitons [57].

Simulations of Eq. (8) for relatively large α and with white noise initial conditions produce V-shaped structures composed of equally spaced, identical bell-shaped solitons that are superimposed on a background of low amplitude ripples [50]. This conclusion is also supported by analytical work [58]. We initially thought that the V-shaped structures could be the differentiated form of the triangular structures we observe in our simulations of Eq. (7). This turns out not to be the case, however: the V-shaped structures occur at much later times than the triangles, and, when integrated, they do not resemble the triangular structures. In addition, the V-shaped structures are found for significantly larger values of α than those for which triangular structures occur. Finally, the V-shaped arrangements of bell-shaped solitons seem not to be transient, unlike the triangular structures we find.

V. DISCUSSION

In this paper, we focused on the effect that the linear dispersive term u_{xxx} has on the patterns produced by oblique-incidence ion bombardment of a solid surface. We found that it can lead to the formation of triangular regions that are traversed by parallel-mode ripples, and these strongly resemble nanostructures observed in many experiments. We included the lowest order nonlinear terms (which are proportional to u_x^2 and u_y^2) in our equation of motion (7). As time passes and the amplitude of the pattern grows, higher order nonlinear terms could begin to modify the behavior of the surface. Quite a number of such terms have been

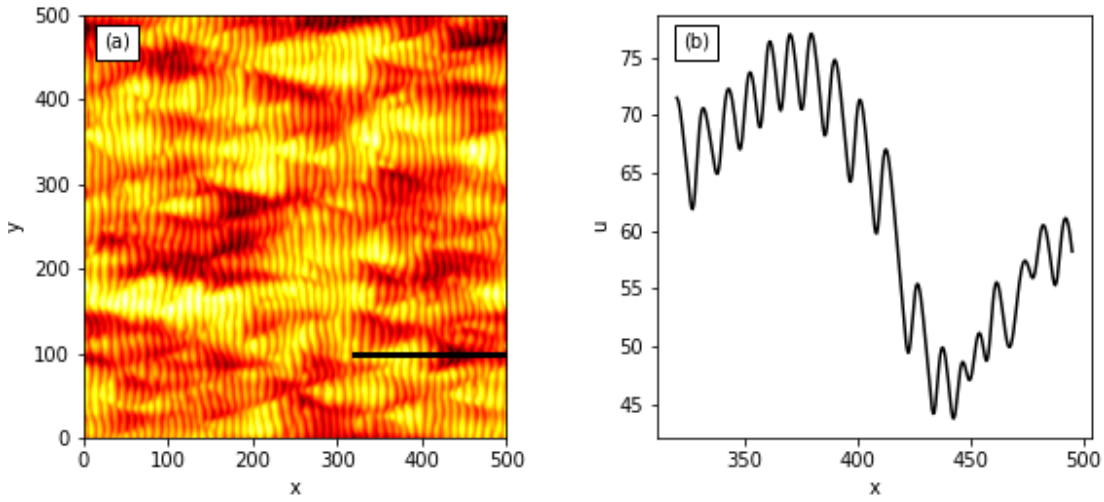

FIG. 17: (a) u vs x and y for $r_1 = 1$, $r_2 = 0$, $\alpha = 3$, and $\beta = 0$ at $t = 76$. The domain size was 500×500. (b) The cross section of the surface taken along the black line shown in (a). The cross section is through one of the triangular structures.

considered and they would likely all influence the surface dynamics at sufficiently long times [11, 12, 48, 49]. However, adding additional terms to the equation of motion would further complicate it, would introduce more dimensionless parameters into a model that already has four, and is accordingly beyond the scope of the present paper.

Perhaps because we included only the lowest order nonlinear terms in our EOM, it does not reproduce all aspects of the experiments. At early times, the triangular structures produced in experiments have cross-sectional profiles that are similar to the ones we find in our simulations (see Fig. 17). However, at later times, the cross section of a triangular structure begins to take on a sawtooth form in some experiments. Such a sawtooth is asymmetric: one of its sides has a significantly larger slope than the other. Our model does not yield this behavior. In addition, the triangular structures produced by our EOM (7) are transient. This transience has not been observed experimentally. This may be because the experimental fluences are not high enough for the triangles to be replaced by perpendicular-mode ripples. However, it is also possible that adding additional nonlinear terms to the EOM would increase the longevity of the triangles and so yield improved agreement with experiment. The experimentally observed triangular structures can also become larger with passing time, and our model fails to reproduce this behavior.

Our equation of motion (7) produces coarsening, i.e., the ripple wavelength increases with time. This increase can be substantial — we find that the wavelength nearly doubles for $\alpha = 1$ in 1D, for example. The ripple wavelength also increases as time passes in experiments that produce triangular structures. Coarsening can also be caused by the so-called conserved Kuramoto-Sivashinsky nonlinearity $\sum_{i=1}^{2}\sum_{j=1}^{2}\lambda_{i,j}^{(2)}\partial_{x_i}^2(\partial_{x_j}u)^2$; here the $\lambda_{i,j}^{(2)}$s are constants [12, 59]. This term is of higher order in both u and the spatial derivatives than the linear dispersive terms u_{xxx} and u_{xyy}, though, and so it is expected to play an important role later in the time evolution than the linear dispersive terms. The cubic nonlinearity u_x^3 also causes coarsening [48, 49] and is of higher order than the linear dispersive terms. In experiments, it is likely that linear dispersion, the conserved Kuramoto-Sivashinsky nonlinearity and the cubic nonlinearity all contribute to ripple coarsening, and that their relative importance changes with time. In all three cases, the ripple wavelength saturates at sufficiently long times, and so the coarsening is interrupted.

The linear dispersive term u_{xxx} is not invariant under the reflection $x \to -x$. Including this term in the EOM has the effect of making the ripples asymmetric, as we saw in Sec. II. There are also nonlinear terms that are not reflectionally symmetric — for example, u_x^3 and $u_x u_{xx}$. If present in the EOM, these terms will also contribute to the asymmetry of the ripples [12, 48]. In addition, these terms alter the propagation velocity of the ripples as the ripple amplitude grows, i.e., they produce nonlinear dispersion [12, 48].

VI. CONCLUSIONS

In this paper, we showed that dispersion can have a crucial effect on the patterns produced by oblique-incidence ion sputtering, even though its effect has almost universally been ignored in the past. Our work yielded four key conclusions:

1. Dispersion can lead to the formation of triangular regions that are traversed by parallel-mode ripples. These structures come in two varieties: those that are raised above the surrounding surface and those that are depressed below it. The raised triangular structures are always oriented in one direction while the depressed triangles are oriented in the opposite direction. We also found that there are a larger number of raised triangles than depressed ones. Triangular structures with precisely these features can be found in many micrographs of ion-sputtered surfaces.

2. If dispersion and transverse smoothing are sufficiently strong, highly ordered ripples can form. Strong effective dispersion can be realized by choosing the angle of ion incidence so that it is just above the critical angle for the formation of parallel-mode ripples. Strong transverse smoothing, however, might be difficult to achieve in practice. Nonetheless, the possibility of exploiting dispersion to produce highly ordered ripples seems a topic worthy of experimental investigation.

3. Dispersion can lead to the formation of protrusions and depressions that are elongated along the projected beam direction even if there is no transverse instability. This may explain why topographies of this kind can form when ion-induced mass redistribution dominates curvature-dependent sputtering.

4. The ripple wavelength increases with time and then saturates as a result of dispersion. Prior research has shown that this behavior — which is known as interrupted coarsening — can also occur due to the presence of nonlinear terms in the equation of motion [12, 48, 49, 59].

ACKNOWLEDGMENTS

R.M.B. is grateful to Adrian Keller for bringing triangular structures on ion-sputtered surfaces to his attention and to Hans Hofsäss and Javier Muñoz-García for useful discussions. The National Science Foundation supported this research through grants DMR-1508745 and DMS-1814941.

---

[1] J. Muñoz-García, L. Vázquez, M. Castro, R. Gago, A. Redondo-Cubero, A. Moreno-Barrado and R. Cuerno, Mater. Sci. Eng. R-Rep. **86**, 1 (2014).

[2] S. Facsko, T. Dekorsy, C. Koerdt, C. Trappe, H. Kurz, A. Vogt, and H. L. Hartnagel, Science **285**, 1551 (1999).

[3] F. Frost, A. Schindler, and F. Bigl, Phys. Rev. Lett. **85**, 4116 (2000).

[4] R. M. Bradley and P. D. Shipman, Phys. Rev. Lett. **105**, 145501 (2010).

[5] P. D. Shipman and R. M. Bradley, Phys. Rev. B **84**, 085420 (2011).

[6] R. M. Bradley and P. D. Shipman, Appl. Surf. Sci. **258**, 4161 (2012)

[7] M. Navez, C. Sella, and D. Chaperot, C. R. Acad. Sci. **254**, 240 (1962).

[8] R. M. Bradley and J. M. E. Harper, J. Vac. Sci. Technol. A **6**, 2390 (1988).

[9] R. Cuerno and A.-L. Barabási, Phys. Rev. Lett. **74**, 4746 (1995).

[10] P. Sigmund, J. Mater. Sci. **8**, 1545 (1973).

[11] M. A. Makeev, R. Cuerno and, A.-L. Barabási, Nucl. Inst. Meth. Phys. Res. B **197**, 185 (2002).

[12] J. Muñoz-García, R. Cuerno and M. Castro, Phys. Rev. B **78**, 205408 (2008).

[13] G. Carter and V. Vishnyakov, Phys. Rev. B **54**, 17647 (1996).

[14] M. Moseler, P. Gumbsch, C. Casiraghi, A. C. Ferrari, and J. Robertson, Science **309**, 1545 (2005).

[15] B. Davidovitch, M. J. Aziz, and M. P. Brenner, Phys. Rev. B **76**, 205420 (2007).

[16] R. M. Bradley and H. Hofsäss, J. Appl. Phys. **120**, 074302 (2016).

[17] H. Hofsäss, K. Zhang, and O. Bobes, J. Appl. Phys. **120**, 135308 (2016).

[18] C. C. Umbach, R. L. Headrick, and K.-C. Chang, Phys. Rev. Lett. **87**, 246104 (2001).

[19] D. Kramczynski, B. Reuscher and H. Gnaser, Phys. Rev. B **89**, 205422 (2014).

[20] S. A. Norris, Phys. Rev. B **85**, 155325 (2012).

[21] S. A. Norris, Phys. Rev. B **86**, 235405 (2012).

[22] M. Castro and R. Cuerno, Appl. Surf. Sci. **258**, 4171 (2012).

[23] A. Moreno-Barrado, M. Castro, R. Gago, L. Vázquez, J. Muñoz-García, A. Redondo-Cubero, B. Galiana, C. Ballesteros, and R. Cuerno, Phys. Rev. B 91, 155303 (2015).

[24] R. M. Bradley, Phys. Rev. B **84**, 075413 (2011).

[25] T. Kawahara, Phys. Rev. Lett. **51**, 381 (1983).

[26] M. Sato and M. Uwaha, Europhys. Lett. **32**, 639 (1995).

[27] C. Misbah and O. Pierre-Louis, Phys. Rev. E **53**, R4318 (1996).

[28] S. M. Cox and P.C. Matthews, J. Comput. Phys. **176**, 430 (2002).

[29] A. Constantinides, "Finite Difference Methods" in *Applied Numerical Methods with Personal Computers*, (McGraw-Hill, New York, 1988), pg. 299.

[30] D. P. Adams, M. J. Vasile, T. M. Mayer, and V. C. Hodges, J. Vac. Sci. Technol. B **21**, 2334 (2003).

[31] D. P. Adams, T. M. Mayer, M. J. Vasile, and K. Archuleta, Appl. Surf. Sci. **252**, 2432 (2006).

[32] J. Grenzer, A. Biermanns, A. Mücklich, S. A. Grigorian, and U. Pietsch, Phys. Status Solidi A **206**, 1731 (2009).

[33] A. Keller and S. Facsko, Materials **3**, 4811 (2010).

[34] G. Carter, M. J. Nobles, F. Paton, J. S. Williams, J. L. Whitton, Rad. Eff. **33**, 65-73 (1977).

[35] A. Keller, S. Facsko, and W. Möller, New J. of Phys. **10**, 063004 (2008).

[36] A. Keller, S. Rossbach, S. Facsko, and W. Möller. Nanotechnology, **19**, 135303 (2008).

[37] A. Metya, D. Ghose, S. A. Mollick, and A. Majumdar, J. Appl. Phys. **111**, 074306 (2012).

[38] D. Chowdhury and D. Ghose, AIP Conf. Proc. **1536**, 353 (2013).

[39] M. Teichmann, J. Lorbeer, B. Ziberi, F. Frost, and B. Rauschenbach, New J. of Phys. **15**, 103029 (2013).

[40] M. Teichmann, J. Lorbeer, F. Frost, and B. Rauschenbach, Nanoscale Res. Lett. **9**, 439 (2014).

[41] D. Chowdhury and D. Ghose, Adv. Sci. Lett. **22**, 105-110 (2016).

[42] R. Gago, M. Jaafar and F. J. Palomares, J. Phys.: Condens. Matter. **30**, 264003 (2018).

[43] A. Lopez-Cazalilla, D. Chowdhury, A. Ilinov, S. Mondal, P. Barman, S. R. Bhattacharyya, D. Ghose, F. Djurabekova, K. Nordlund, and S. Norris, J. Appl. Phys. **123**, 235304 (2018).

[44] A. Keller, M. Nicoli, S. Facsko, and R. Cuerno, Phys. Rev. E **84**, 015202(R) (2011).

[45] S. A. Norris, M. P. Brenner, and M. J. Aziz, J. Phys. Condens. Matter, **21**, 224017 (2009).

[46] S. A. Norris, J. Samela, L. Bukonte, M. Backman, F. Djurabekova, K. Nordlund, C. S. Madi, M. P. Brenner, and M. J. Aziz, Nature Commun. **2**, 276 (2011).

[47] M. P. Harrison and R. M. Bradley, Phys. Rev. B **89**, 245401 (2014).

[48] D. A. Pearson and R. M. Bradley, J. Phys.: Cond. Matt. **27**, 015010 (2015).

[49] M. P. Harrison, D. A. Pearson, and R. M. Bradley, Phys. Rev. E **96**, 032804 (2017).

[50] K. Indireshkumar and A. L. Frenkel, Phys. Rev. E **55**, 1174 (1997).

[51] V. E. Zakharov and E. A. Kuznetsov, Zh. Eksp. Teor. Fiz. **66**, 594 (1974) [Sov. Phys. JETP **39**, 285 (1974)].

[52] E.W. Laedke and K.H. Spatschek, J. Plasma Phys. **28**, 469 (1982).

[53] E. Infeld, J. Plasma Phys. **33**, 171 (1985).

[54] E. Infeld and P. Frycz, J. Plasma Phys. **37**, 97 (1987).

[55] E. Infeld and P. Frycz, J. Plasma Phys. **41**, 441 (1989).

[56] M.A. Allen, G. Rowlands, J. Plasma Phys. **50**, 431 (1993).

[57] P. Frycz and E. Infeld, Phys. Rev. Lett. **63**, 384 (1989).

[58] S. Saprykin, E. A. Demekhin and S. Kalliadasis, Phys. Rev. Lett. **63**, 224101 (2005).

[59] J. Muñoz-García, M. Castro and R. Cuerno, Phys. Rev. Lett. **96**, 086101 (2006).